Hindawi
Geofluids
Volume 2022, Article ID 1932642, 9 pages
https://doi.org/10.1155/2022/1932642

Research Article

Experimental Research on Fracture Characteristics of Reactive Powder Concrete in Different Volume Content of Steel Fiber

Wenzhen Wang,[1] Haixiao Lin ,[1,2] Xiaogang Wu,[1] Yuyao Zhao,[1] Ziyu Hu,[1] Pengshuai Wang,[1] and Menglong Zhou[1]

[1]*School of Civil Engineering, Henan Polytechnic University, Jiaozuo, 454000 Henan, China*
[2]*Henan Key Laboratory of Underground Engineering and Disaster Prevention, Henan Polytechnic University, Jiaozuo, 454000 Henan, China*

Correspondence should be addressed to Haixiao Lin; hpulhx@hpu.edu.cn

Received 24 February 2022; Revised 24 April 2022; Accepted 6 May 2022; Published 19 May 2022

Academic Editor: Su Shan-Jie

The fracture characteristics of reactive powder concrete in different volume content of steel fiber are researched in this paper, combining with the photoelastic coating method and the mathematical analytical software MATLAB. More precisely, the wholly integrated initiation, stable propagation, and final failure stages of precast cracks in three-point bending specimens of reactive powder concrete in different volume content of steel fiber are directly recorded and systematically analyzed. Besides, the photoelastic fringe distribution graphs from the vicinity of the precast cracks of specimens are obtained. Based on the experimental results and fracture mechanics theory, the mechanical property of reactive powder concrete, fracture energy, ductility index, initial fracture toughness, and unstable fracture toughness are quantitatively and qualitatively analyzed. The research achievements indicate that there is a stable crack propagation process before the instability failure of the three-point bending beam specimen of reactive powder concrete. The fracture process of the structure includes three stages, namely, the crack initiation, stable propagation, and instability failure. The order of the photoelastic fringe, critical effective crack length, crack initiation load, and maximum load of test parameters in the three-point bending beam specimen of reactive powder concrete increases with the increase of the fiber volume ratio. Based on the numerical treatment for the whole curves of each specimen group, the softening curve and the double fracture parameters of reactive powder concrete are obtained. Besides, the calculated critical effective joint length, initiation toughness, toughness increment, and unstable fracture toughness increase with the increase of the steel fiber volume ratio, by analyzing the measured initiation load, maximum load, and critical effective joint length. The research results can be treated as an important basis and reference for the engineering design and safety assessment of reactive powder concrete.

1. Introduction

Reactive powder concrete is a new type of cement-based composite material with ultra-high strength, high durability, and low brittleness. It was first developed by French Richard and others in the 1990s [1, 2]. Based on the most compact packing theory, reactive powder concrete removes the coarse aggregate, takes fine quartz sand as the aggregate, and adds a high efficiency water reducing agent and an appropriate amount of steel fiber, thereby improving the compressive strength and toughness of concrete by reducing internal defects [3, 4]. Compared with ordinary concrete, reactive powder concrete has higher specific strength, which effectively reduces the dead weight of the structure and saves the amount of materials [5, 6]. Besides, reactive powder concrete has the characteristics of high brittleness of ordinary concrete and achieves the effect of strengthening and toughening by adding fiber [7, 8].

At present, reactive powder concrete is becoming a hot research issue at home and abroad in recent years, because of its superior performance [9, 10]. According to the research results of Bonneau et al. [11], the reactive powder

Table 1: Serial number of specimens.

Specimen number	0	1	2	3
Volume content of steel fiber	0%	1.0%	2.0%	3.0%
The number of specimens	3(0-1, 0-2, 0-3)	3(1-1, 1-2, 1-3)	3(2-1, 2-2, 2-3)	3(3-1, 3-2, 3-3)

(a) UJZ-15 mortar blending machine

(b) Digital control magnetic vibrating table

(c) YH-20B standard constant temperature and humidity curing box

(d) HJ-84 concrete accelerated curing box

Figure 1: Testing equipment.

(a) Overall instrument picture

(b) Local instrument picture

Figure 2: Composition of reflective photoelastic instrument.

concrete has ultra-high compressive strength and durability, compared with ordinary concrete through experimental research. Cheyrezy et al. [12] studied the variation law of pore diameter and porosity of reactive powder concrete under different curing systems and obtained the conclusion that high-temperature autoclave curing significantly reduces

(a) $P = 0.73$ kN

(b) $P = 1.67$ kN

Figure 3: Crack propagation displayed by coatings (specimen 0-2).

(a) $P = 2.16$ kN

(b) $P = 4.47$ kN

Figure 4: Crack propagation displayed by coatings (specimen 1-2).

the porosity of reactive powder concrete. Ahmad et al. [13] studied the influence law of three key factors on the performance of reactive powder concrete by optimizing sand gradation, namely, cement content, water binder ratio, and silica fume. The test results indicate that three key factors have a significant impact on the fluidity and strength of reactive powder concrete, and the regression equation of mechanical properties of reactive powder concrete is obtained.

It is obvious that fracture characteristics of reactive powder concrete in different volume content of steel fiber are not researched systematically. Therefore, the experimental research on fracture characteristics of reactive powder concrete in different volume content of steel fiber is researched in this paper. The research results can be treated as an important basis and reference for the engineering design and safety assessment of reactive powder concrete.

2. Preparation of Experimental Specimens

In this paper, three-point bending beam specimens are tested in the laboratory. According to the change of the fiber volume content, the specimens are divided into four groups, with three specimens in each group. The volume content of steel fiber in the specimen is 0%, 1.0%, 2.0%, and 3.0%. Meanwhile, the corresponding numbers are 0, 1, 2, and 3. The numbers of three-point bending beam specimens are shown in Table 1.

The specific preparation method and test steps of the three-point bending beam specimen are set. (1) According to the mixing proportion, the raw materials are weighed, and the cement, silica fume, quartz powder, and quartz sand are poured into the mortar mixer. (2) When adding steel fiber, the steel fiber is slowly and evenly sprinkled into the mixer during the mixing process. (3) The half consumption

(a) $P = 2.41$ kN

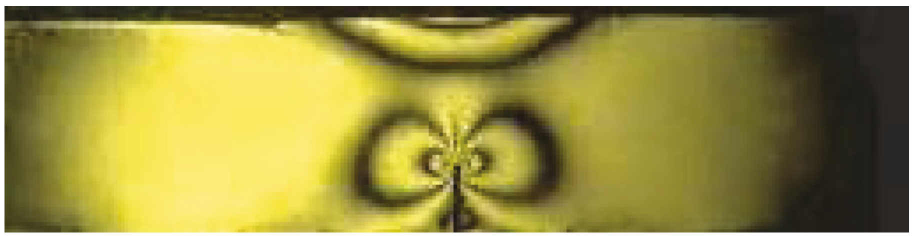

(b) $P = 4.82$ kN

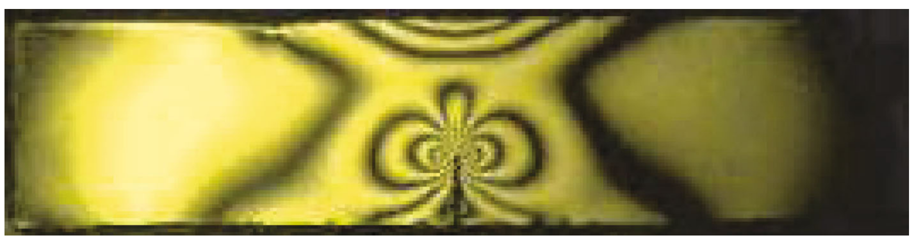

(c) $P = 7.29$ kN

Figure 5: Crack propagation displayed by coatings (specimen 2-1).

of water dissolved in a water-reducing agent is added and stirred for about three minutes. (4) The other half consumption of the water is poured and stirred for about six minutes. (5) The mixed reactive powder concrete is poured into the triple mold placed on the shaking table coated with a release agent in advance. Half of the reactive powder concrete is poured in the mold firstly, and the shaking table is started, vibrating for one minute; then, the other half of the reactive powder concrete is poured and undergoes vibration for one minute. (6) For the initial cracks of the specimen, the grooves are set in advance inside the test partition, and the thin iron sheet is inserted vertically into the grooves in advance when the steel fiber concrete is poured. After pouring and curing the test piece for more than 24 hours, the thin iron sheet is pulled out to form a reserved seam. (7) After the reactive powder concrete specimens are formed, the reactive powder concrete specimens are moved into the curing room (temperature $20 \pm 3^{\circ}$C, relative humidity above 90%), and the mold is removed after the specimens are cured for 24 hours. Then, the reactive powder concrete specimens are immediately placed in a $90 \pm 2^{\circ}$C hot water curing box for curing. Finally, the reactive powder concrete specimens are taken out after 72 hours of heat curing, and then, the specimens are cooled to room temperature.

The key equipment employed to test the reactive powder concrete includes the UJZ-15 mortar blending machine, digital control magnetic vibrating table (the vibration frequency is 2860 times/min), YH-20B standard constant temperature and humidity curing box, and HJ-84 concrete accelerated curing box, shown in Figure 1.

3. Photoelastic Patch Method Experiment

3.1. Experimental Principle. The photoelastic patch method extends the traditional photoelastic model test to measure the surface strain field distribution on a 2D and 3D opaque model made of structural material [14]. And the elastic and plastic strains of the structure surface are measured by the photoelastic patch method. The patch is a thin layer of birefringent material, deforming with the deformation of the plane or curved structural surface of the structure, which is used as a sensing element to analyze the test result [15].

Therefore, the photoelastic patch method is employed to directly observe the whole process of prefabricated crack initiation, stable expansion, and instability failure of the three-point bending beam specimen of reactive powder concrete, which is of great importance for further research on the fracture mechanism and fracture characteristics of steel fiber-reinforced concrete [16].

3.2. Experimental Equipment. The experiment adopts the Photoelastic Division patch produced by the Measurements Group Inc., and the thickness of the patch is 3.02 ± 0.05 mm. The photoelastic patch is closely attached to the surface of the object to be tested, in order to accurately reflect the

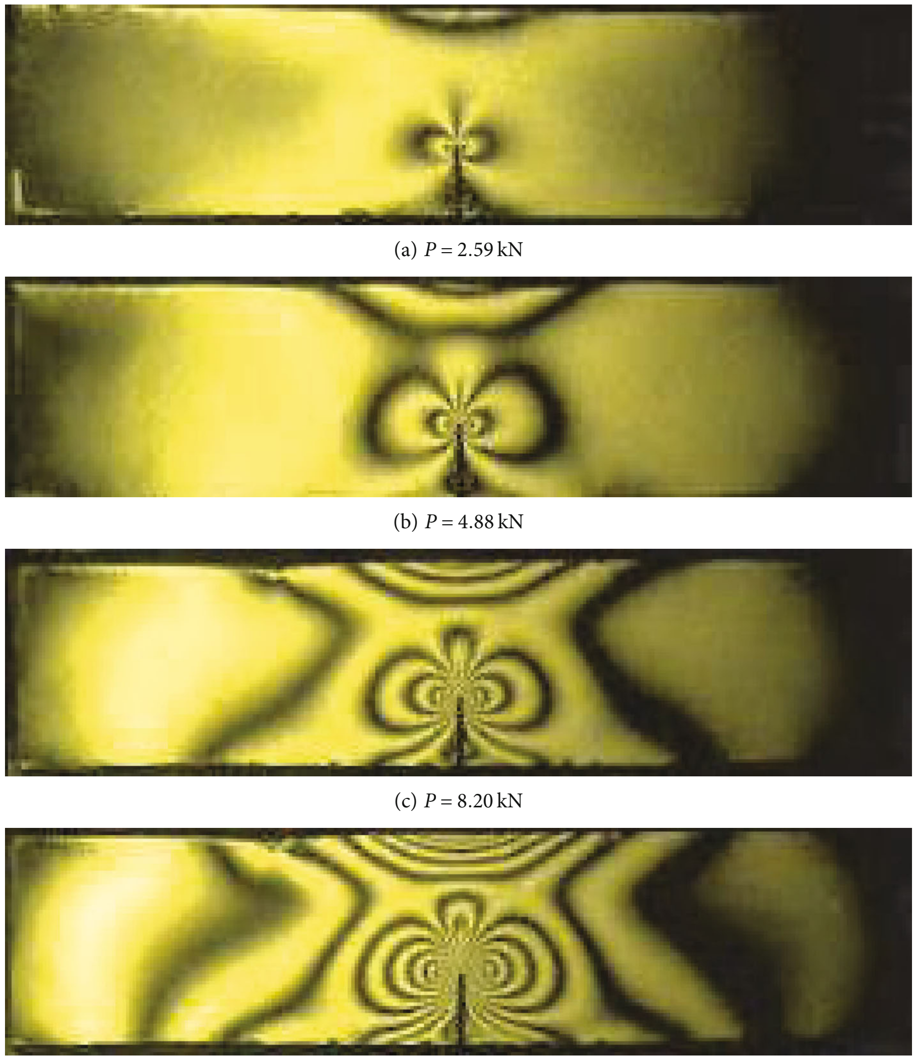

(a) $P = 2.59$ kN

(b) $P = 4.88$ kN

(c) $P = 8.20$ kN

(d) $P = 10.41$ kN

Figure 6: Crack propagation displayed by coatings (specimen 3-3).

stress state of the object [17]. A whole patch is attached to the three-point bending beam specimen of the reactive powder concrete and a crack of the same length as the specimen is prefabricated in the middle of the patch. The sticking steps are set: (1) filling the surface of the test piece and grinding it with sandpaper to achieve the superior flatness of test piece; (2) mixing the viscous material in proportion and spreading it evenly on the surface of the prepared test piece; (3) pasting the patch; (4) after the patch is pasted on the test piece, squeezing the glue evenly and smoothly sealing the glue at the edge of the patch.

The key equipment employed in the experiment includes the loading equipment of a servo fatigue testing machine and the corresponding computer data acquisition system. The maximum load range of the testing machine is 200 kN, and the displacement control is adopted in the loading control method. The reflective photoelastic instrument consists of a polarizing environment, a light source, a digital camera, a filter, a bracket, and a device fixing table, shown in Figure 2.

3.3. Experimental Results. The isoline fringe patterns displayed by the photoelastic patch method under various loads are photographed for each specimen in the test. The test specimens are tested for the photoelastic patch in the process of crack initiation and crack expansion under various loads. The images of specimen 0-2, specimen 1-2, specimen 2-1, and specimen 3-3 are shown in Figures 3, 4, 5, and 6, respectively.

The steel fibers prevent the development of defects such as microcracks in the concrete, delay the occurrence of initial cracks, and improve the initial crack strength in the reactive powder concrete specimens mixed with steel fibers. Although the matrix has been cracked, the steel fibers bridging at the cracks begin to bear the stress transmitted by the interface between the reactive powder concrete matrix and the steel fiber, so that the specimens continue to bear larger loads and produce elastic-plastic deformation.

With the increase of the load, the length and width of the microcracks on the surface of the reactive powder concrete continues to increase, and some new microcracks occur near

Table 2: Related indexes of softening curve for reactive powder concrete.

Specimen number	V_f	f_{ts} (MPa)	f_t (MPa)	λ	G_f (KJ/m^2)	ω_0 (mm)	α	β
0-1	0	9.69	8.24	8	0.150	0.146	0.710	-0.002
0-2					0.150	0.146		
0-3					0.154	0.149		
Average value					0.151	0.147		
1-1	1%	16.80	14.28	7	13.765	7.184	0.782	-0.005
1-2					10.209	5.328		
1-3					10.310	5.381		
Average value					11.428	5.964		
2-1	2%	29.64	24.68	6	21.061	5.784	0.942	-0.025
2-2					25.525	7.010		
2-3					18.552	5.095		
Average value					21.713	5.963		
3-1	3%	34.54	29.36	5	23.029	4.685	0.974	-0.025
3-2					30.433	6.191		
3-3					25.886	5.266		
Average value					26.449	5.381		

Table 3: Fracture energy and related indexes of reactive powder concrete.

Specimen number	P_{max} (kN)	δ_{max} (mm)	mg (N)	G_f (KJ × m^{-2})	D_u (m^{-1})	l_{ch} (m)	f_t (MPa)
0-1	1.59	0.21	5.96	0.150	0.094	0.069	8.24
0-2	1.67	0.20	5.99	0.150	0.090	0.066	
0-3	1.49	0.23	6.01	0.154	0.103	0.076	
Average value	1.58	0.21	5.99	0.151	0.096	0.071	
1-1	4.64	10.21	6.08	13.765	2.967	0.727	14.28
1-2	4.47	7.86	6.10	10.209	2.284	0.560	
1-3	4.38	8.10	6.12	10.310	2.354	0.577	
Average value	4.50	8.72	6.10	11.428	2.535	0.622	
2-1	7.29	7.78	6.25	21.061	2.889	0.237	24.68
2-2	8.03	8.93	6.17	25.525	3.179	0.261	
2-3	6.67	7.24	6.22	18.552	2.781	0.228	
Average value	7.33	7.98	6.21	21.713	2.950	0.242	
3-1	9.67	6.54	6.36	23.029	2.382	0.138	29.36
3-2	12.00	7.26	6.34	30.433	2.536	0.147	
3-3	10.41	6.96	6.39	25.886	2.487	0.144	
Average value	10.69	6.92	6.36	26.449	2.468	0.143	

the original cracks. These new cracks continue to expand and connect with the original cracks to form the key failure cracks. When the load increases to the peak value, the cracks on the surface of the reactive powder concrete expand widely. Even if the load does not increase, the cracks continue to expand and start from close to the peak value. Meanwhile, the sound of the steel fibers being pulled out from the specimen is clearly heard in the test.

After entering the residual stress stage after the peak, the deflection increases greatly and the load decreases slowly. When the specimen loses its bearing capacity, a small amount of steel fibers is still connected in the section. Besides, the fiber occlusion area extends to the upper edge, and the fracture is rough. The steel fibers at the fracture of the specimens are pulled out due to the bond failure, and the phenomenon of fiber breaking rarely occurs.

4. Fracture Mechanism of Reactive Powder Concrete Based on Double-K Fracture Criterion

4.1. Determination of Double-K Fracture Parameters. Because there is a stable crack propagation stage before the unstable fracture of concrete, the actual crack length a of the specimen before the unstable fracture is greater than the prefabricated joint length a_0. If the stable crack propagation length Δa_c before the unstable fracture is recorded, then

$$a_c = a_0 + \Delta a_c. \quad (1)$$

According to the linear progressive superposition principle, the critical effective crack length a_c is calculated by calculating the linear elastic fracture mechanical equation. When the external load P of the three-point bending beam reaches the maximum load $P_{\max}$, the corresponding critical effective crack length a_c is determined by the following equation:

$$\mathrm{CMOD}_c = \frac{6P \max Sa_c}{th^2 E} V_1(\alpha), \quad (2)$$

where CMOD_c is the crack opening displacement; E is the elastic modulus; S, t, and h are beam span, beam thickness, and beam height, respectively; the expression of $V_1(\alpha)$ is $V_1(\alpha) = 0.76 - 2.28\alpha + 3.87\alpha^2 - 2.04\alpha^3 + 0.66/(1-\alpha)^2$; and H_0 is the blade thickness.

The elastic modulus is calculated by equation (3), according to the initial elastic flexibility of a curve.

$$E = \frac{24}{thc_i} a_0 V_1(\alpha_0). \quad (3)$$

There is a stable expansion stage of key cracks before the unstable expansion of concrete. When the crack opening displacement ω is less than ω_0, the stress is transferred, which is called the closing force. The stress intensity factor of the crack tip is

$$K_I = K_I^P - K_I^\sigma, \quad (4)$$

where K_I^P is the stress intensity factor caused by concentrated force P.

The three-point bending beam specimen K_I^P is directly calculated by the following linear elastic fracture mechanical equation:

$$K_I^P = \frac{3PS}{2h^2 t} \sqrt{a} f_2\left(\frac{a}{h}\right), \quad (5)$$

where

$$f_2\left(\frac{a}{h}\right) = \frac{1.99 - (a/h)(1-a/h)\left[2.15 - 3.93(a/h) + 2.7(a/h)^2\right]}{(1+2(a/h))(1-a/h)^{3/2}}. \quad (6)$$

The calculation equation (7) of the stress intensity factor generated by the closing force is obtained.

$$K_I^\sigma = \int_{a_0}^{a} 2\sigma(x) F\left(\frac{x}{a}, \frac{a}{h}\right) / \sqrt{\pi a} dx. \quad (7)$$

An approximate solution form of integral formula (7) is

$$K_{Ic}^c = -Z\left(U_e, \frac{V_0}{V_c}\right) \frac{2P_e}{\sqrt{\pi a_c}} F(U_e, V_c). \quad (8)$$

It is obtained by equation (4) that when the crack is in the critical state of crack initiation, equation (9) is satisfied.

$$K_{Ic}^{ini} = K_{Ic}^{un} - K_{Ic}^c. \quad (9)$$

The instability fracture toughness is obtained by substituting the maximum load $P_{\max}$ measured in the test and the a_c calculated by equation (2) into equation (5). The crack initiation toughness is the stress intensity factor corresponding to the load P_{ini} at the crack initiation of concrete. a_c is substituted into equation (8) to obtain K_{Ic}^c and then substituted into equation (9) to obtain crack initiation toughness.

4.2. Application Results of Fracture Criteria. According to the above derivation, α and β under each parameter are obtained, shown in Table 2.

Taking α and β as the function of fiber volume content V_f, the polynomial model is adopted and fitted with MATLAB software. The fitting results are obtained in the following equations:

$$\alpha = -1.011 V_f^2 + 1.254 V_f + 0.699, \quad (10)$$

$$\beta = 0.085 V_f^2 - 0.114 V_f. \quad (11)$$

The relationship of $f_t = 0.85 f_{ts}$ is satisfied in steel fiber-reinforced concrete with different fiber volume content. The $\sigma - \omega$ softening curve is obtained, and the softening curve of reactive powder concrete without fiber is the most concave. The variations of the initiation load P_{ini} and maximum load $P_{\max}$ with fiber volume content are obtained, shown in Table 3.

The initiation load P_{ini} and maximum load $P_{\max}$ of each group of reactive powder concrete specimens gradually increase with the increase of fiber volume content.

4.2.1. Fracture Energy G_f. The fracture energy of the reactive powder concrete specimen without fiber is $0.151\,\mathrm{KJ{\cdot}m^{-2}}$. After the fiber is added, the fracture energy increases by an order of magnitude. Taking the specimen with the lowest fiber content $V_f = 1.0\%$ as an example, the fracture energy reaches $11.428\,\mathrm{KJ{\cdot}m^{-2}}$, which is 76 times higher than that at $V_f = 0\%$. Since the fracture energy increases with the increase of fiber content, the fracture energy of the reactive powder concrete specimen at $V_f = 2.0\%$ and $V_f = 3.0\%$ is respectively 1.9 times and 2.3 times that at $V_f = 1\%$.

4.2.2. Ductility Index D_u. The ductility index D_u is defined as the ratio the fracture energy G_f and load peak $p_{\max}$ in deflection curve.

$$D_u = \frac{G_f}{P_{\max}}. \quad (12)$$

The ductility index is employed to characterize the deformation resistance of reactive powder concrete. The greater the ductility index, the stronger the deformation resistance of the material. The ductility index of the reactive powder concrete without fiber is $0.096\,\mathrm{m}^{-1}$. After the fiber is added, the ductility index increases in the order of magnitude. Taking the specimen with the lowest fiber content $V_f = 1.0\%$ as an example, the ductility index reaches $2.535\,\mathrm{m}^{-1}$, which is 26 times higher than that at $V_f = 0\%$.

The effect of steel fiber on improving the ductility index of reactive powder concrete is obvious. When the fiber content exceeds 1%, the increase of the ductility index is small. The ductility index of the reactive powder concrete at $V_f = 2.0\%$ is $2.950\,\mathrm{m}^{-1}$, which is $0.415\,\mathrm{m}^{-1}$ compared with that at $V_f = 1\%$. The ductility index of the reactive powder concrete reaches the maximum at $V_f = 2.0\%$. When $V_f = 3.0\%$, the ductility index decreases with the increase of the fiber volume content, and the ductility index is $2.468\,\mathrm{m}^{-1}$. Because the peak strength of the reactive powder concrete increases with the increase of fiber volume content, especially at $V_f = 3.0\%$, the peak load reaches the maximum. However, the brittleness of the material increases with the increase of strength, and the $P-\delta$ curve becomes significantly steeper.

4.2.3. Characteristic Length l_{ch}. The characteristic length L is employed to characterize the brittleness of concrete, which is defined in the following equation:

$$l_{ch} = \frac{G_f \times E}{f_t^{\,2}}, \quad (13)$$

where E is the elastic modulus of concrete and f_t is the tensile strength of concrete.

The smaller the characteristic length, the greater the brittleness of the material. The characteristic length of each test piece is shown in Table 3. The characteristic length of the reactive powder concrete without fiber is 0.071 m. After the fiber is added, the characteristic length increases. Taking the specimen with fiber content $V_f = 1.0\%$ as an example, the characteristic length reaches 0.622 m. The characteristic length decreases with the increase of the fiber content. Besides, the characteristic length of reactive powder concrete is 0.242 m and 0.143 m at $V_f = 2.0\%$ and $V_f = 3.0\%$, respectively.

5. Conclusions

The fracture performance of the reactive powder concrete is experimentally studied by the fracture test of a precast cracked three-point bending beam with different fiber volume content in this paper, and the conclusions are obtained as follows.

(1) The whole process of crack generation and propagation of the three-point bending beam specimen of reactive powder concrete is obtained by the photoelastic patch method. Before the instability failure of the three-point bending beam specimen of the reactive powder concrete, there is a stable crack propagation process. The fracture process of the structure includes three stages, namely, the crack initiation, stable propagation, and instability failure. Besides, the order of photoelastic fringe, the critical effective crack length, the crack initiation load, and the maximum load of test parameters increase with the increase of fiber content in the test image of the beam specimen of reactive powder concrete

(2) According to the stripe image obtained by the photoelastic patch method, the stress distribution information of the three-point bending beam specimen of reactive powder concrete in the whole field is obtained, and the characteristics of stress distribution are intuitively displayed. By analyzing the test results, it is obvious that the stress distribution has obvious rationality and regularity. Through the numerical treatment of the whole curves of each group of specimens, the softening curve of reactive powder concrete is obtained

(3) Based on the test data in this paper, the double fracture parameters of reactive powder concrete specimens are obtained. Besides, the fracture energy, ductility index, and characteristic length of reactive powder concrete specimens with different fiber volume content are obtained. Besides, the calculated critical effective joint length, initiation toughness, toughness increment, and unstable fracture toughness increase with the increase of the steel fiber volume ratio, by analyzing the measured initiation load, maximum load, and critical effective joint length

Data Availability

The data used to support the findings of this study are included within the article.

Conflicts of Interest

The authors declare that they have no conflicts of interest.

Acknowledgments

This work was supported by the Science and Technology Project of Henan Province (222102320381), the Foundation for Higher Education Key Research Project by Henan Province (22A130002), the Project of Henan Key Laboratory of Underground Engineering and Disaster Prevention (Henan Polytechnic University), the Ph.D. Programs Foundation of Henan Polytechnic University (B2021-57), the Postdoctoral Research Projects of Henan Province, the Research and Practice Project of Higher Educational and Teaching Reformation of Henan Province (2021SJGLX376), the Virtual

Simulation Experiment Teaching Project of Henan Province, and the Research and Practice Project of Educational and Teaching Reformation of Henan Polytechnic University (2021JG020 and 2019JG074).

References

[1] R. Contamine, A. S. Larbi, and P. Hamelin, "Contribution to direct tensile testing of textile reinforced concrete (TRC) composites," *Materials Science and Engineering A*, vol. 528, no. 29-30, pp. 8589–8598, 2011.

[2] T. Suwan, P. Jitsangiam, and P. Chindaprasirt, "Influence of nano-silica dosage on properties of cement paste incorporating with high calcium fly ash," *Key Engineering Materials*, vol. 4874, pp. 9–13, 2020.

[3] J. Liu, Y. Xue, Q. Zhang, H. Wang, and S. Wang, "Coupled thermo-hydro-mechanical modelling for geothermal doublet system with 3D fractal fracture," *Applied Thermal Engineering*, vol. 200, article 117716, 2022.

[4] Z. Z. Cao, Y. Wang, H. X. Lin, Q. Sun, X. G. Wu, and X. S. Yang, "Hydraulic fracturing mechanism of rock mass under stress-damage-seepage coupling effect," *Geofluids*, vol. 2022, Article ID 5241708, 2022.

[5] N. Zabihi and M. Hulusi Ozkul, "The fresh properties of nano silica incorporating polymer-modified cement pastes," *Construction and Building Materials*, vol. 168, no. 7, pp. 570–579, 2018.

[6] J. Puentes, G. Barluenga, and I. Palomar, "Effects of nano-components on early age cracking of self-compacting concretes," *Construction and Building Materials*, vol. 73, no. 6, pp. 89–96, 2014.

[7] Y. Xue, J. Liu, P. G. Ranjith, Z. Zhang, F. Gao, and S. Wang, "Experimental investigation on the nonlinear characteristics of energy evolution and failure characteristics of coal under different gas pressures," *Bulletin of Engineering Geology and the Environment*, vol. 81, no. 1, article 38, 2022.

[8] J. Hegger and S. Voss, "Investigations on the bearing behaviour and application potential of textile reinforced concrete," *Engineering Structures*, vol. 30, no. 7, 2008.

[9] F. Parisio, V. Vilarrasa, and L. Laloui, "Hydro-mechanical modeling of tunnel excavation in anisotropic shale with coupled damage-plasticity and micro-dilatant regularization," *Rock Mechanics and Rock Engineering*, vol. 51, no. 12, pp. 3819–3833, 2018.

[10] P. Hou, Y. Xue, F. Gao et al., "Effect of liquid nitrogen cooling on mechanical characteristics and fracture morphology of layer coal under Brazilian splitting test," *International Journal of Rock Mechanics and Mining Sciences*, vol. 151, article 105026, 2022.

[11] O. Bonneau, M. Laehemi, and E. Dallaire, "Mechanical properties and durability of two industrial reactive powder concretes," *ACI Materials Journal*, vol. 94, no. 4, pp. 286–290, 1997.

[12] M. Cheyrezy, V. Maret, and L. Frouin, "Microstructural analysis of RPC (reactive powder concrete)," *Cement and Concrete Research*, vol. 25, no. 7, pp. 1491–1500, 1995.

[13] S. Ahmad, A. Zubair, and M. Maslehuddin, "Effect of key mixture parameters on flow and mechanical properties of reactive powder concrete," *Construction and Building Materials*, vol. 99, pp. 73–81, 2015.

[14] Y. Xue, J. Liu, X. Liang, S. Wang, and Z. Ma, "Ecological risk assessment of soil and water loss by thermal enhanced methane recovery: numerical study using two-phase flow simulation," *Journal of Cleaner Production*, vol. 334, article 130183, 2022.

[15] Z. Z. Cao, Y. F. Xue, H. Wang, J. R. Chen, and Y. L. Ren, "The non-Darcy characteristics of fault water inrush in karst tunnel based on flow state conversion theory," *Thermal Science*, vol. 25, no. 6 Part B, pp. 4415–4421, 2021.

[16] A. Madadi, H. Eskandari-Naddaf, and M. N. Nejad, "Evaluation of bond strength of reinforcement in concrete containing fibers, micro-silica and nano-silica," *Journal of Stress Analysis*, vol. 3, no. 1, pp. 11–19, 2018.

[17] X. Z. Li, G. Y. Luo, and Z. S. Chen, "The mechanism of deformation and water conduction of fault due to excavation in water inrush in underground engineering," *Chinese Journal of Geotechnical Engineering*, vol. 6, pp. 695–700, 2002.